Mon. Not. R. Astron. Soc. **402,** 895–902 (2010) doi:10.1111/j.1365-2966.2009.15973.x

# *HST*/NICMOS Paschen-$\alpha$ Survey of the Galactic Centre: Overview

Q. D. Wang,[1⋆] H. Dong,[1] A. Cotera,[2] S. Stolovy,[3] M. Morris,[4] C. C. Lang,[5] M. P. Muno,[6] G. Schneider[7] and D. Calzetti[1]

[1]*Department of Astronomy, University of Massachusetts, Amherst, MA 01003, USA*
[2]*SETI Institute, 515 North Whisman Road, Mountain View, CA 94043, USA*
[3]*Spitzer Science Center, California Institute of Technology, Mail Code 220-6, 1200 East California Boulevard, Pasadena, CA 91125, USA*
[4]*Department of Physics and Astronomy, University of California, Los Angeles, CA 90095, USA*
[5]*Department of Physics and Astronomy, University of Iowa, Iowa City, IA 52245, USA*
[6]*Space Radiation Laboratory, California Institute of Technology, Pasadena, CA 91125, USA*
[7]*Steward Observatory, The University of Arizona, Tucson, AZ 85721, USA*

Accepted 2009 November 2. Received 2009 October 29; in original form 2009 September 22

**ABSTRACT**

We have recently carried out the first wide-field hydrogen Paschen-$\alpha$ line imaging survey of the Galactic Centre using the Near Infrared Camera and Multi-Object Spectrometer (NICMOS) instrument aboard the *Hubble Space Telescope*. The survey maps out a region of 2253 pc$^2$(416 arcmin$^2$) around the central supermassive black hole (Sgr A*) in the 1.87 and 1.90 μm narrow bands with a spatial resolution of ∼0.01 pc (0.2 arcsec full width at half-maximum) at a distance of 8 kpc. Here, we present an overview of the observations, data reduction, preliminary results and potential scientific implications, as well as a description of the rationale and design of the survey. We have produced mosaic maps of the Paschen-$\alpha$ line and continuum emission, giving an unprecedentedly high-resolution and high-sensitivity panoramic view of stars and photoionized gas in the nuclear environment of the Galaxy. We detect a significant number of previously undetected stars with Paschen-$\alpha$ in emission. They are most likely massive stars with strong winds, as confirmed by our initial follow-up spectroscopic observations. About half of the newly detected massive stars are found outside the known clusters (Arches, Quintuplet and Central). Many previously known diffuse thermal features are now resolved into arrays of intriguingly fine linear filaments indicating a profound role of magnetic fields in sculpting the gas. The bright spiral-like Paschen-$\alpha$ emission around Sgr A* is seen to be well confined within the known dusty torus. In the directions roughly perpendicular to it, we further detect faint, diffuse Paschen-$\alpha$ emission features, which, like earlier radio images, suggest an outflow from the structure. In addition, we detect various compact Paschen-$\alpha$ nebulae, probably tracing the accretion and/or ejection of stars at various evolutionary stages. Multiwavelength comparisons together with follow-up observations are helping us to address such questions as where and how massive stars form, how stellar clusters are disrupted, how massive stars shape and heat the surrounding medium, how various phases of this medium are interspersed and how the supermassive black hole interacts with its environment.

**Key words:** circumstellar matter – stars: formation – Galaxy: centre – infrared: stars.

## 1 INTRODUCTION

The Galactic centre (GC) is a unique laboratory for a detailed study of star formation and its impact on the nuclear environment of galaxies. Because of its proximity, the GC can be imaged at resolutions more than 100 times better than the nearest galaxies like our own (e.g. the Andromeda galaxy). This unmatched high-resolution capability is particularly important to the study of the formation and destruction processes of stellar clusters as well as the overall population of massive stars in such an environment. Indeed, the GC is known to host three very massive clusters the Arches and Quintuplet clusters, as well as the central parsec cluster surrounding Sgr A*; ages ∼2–7 × 10$^6$ yr, masses ∼3 × 10$^4$ M$_\odot$ each; (e.g. Cotera et al. 1996; Serabyn, Shupe & Figer 1998; Figer et al. 1999, 2002; Genzel et al. 2003), which are responsible for about 5 per cent of the total Lyman continuum flux for the Galaxy, in less than 0.01 per cent of its volume. Massive stars are known to exist outside the

⋆E-mail: wqd@astro.umass.edu

clusters (Cotera et al. 2006); however, locating these important stars has been sporadic and incomplete (e.g. Muno et al. 2006a; Mauerhan, Muno & Morris 2007; Mauerhan et al. 2009). These isolated massive stars may have formed individually or in small groups, although the extreme conditions in the GC make this mode of star formation unusually difficult. They may also have been spun out of the clusters due to their internal dynamics. This process is expected to be accelerated by the strong external tidal force in the GC (Kim, Morris & Lee 1999).

The star formation process depends critically on the interplay of massive stars with the interstellar medium (ISM). Massive stars release large amounts of ultraviolet radiation. They also produce strong stellar winds throughout their short lives and die in supernova explosions. Such energetic stellar output dramatically shapes the morphology of the ISM, as is revealed in existing radio, mid-infrared and X-ray maps (fig. 1; e.g. Yusef-Zadeh, Morris & Chance 1984; Yusef-Zadeh et al. 2002; Wang, Gotthelf & Lang 2002; Wang, Dong & Lang 2006; Muno et al. 2009). Perhaps the best-known example of this is the Radio Arc region which surrounds the Arches and Quintuplet clusters: a collection of arc-like thermal filaments, synchrotron-bright non-thermal linear filaments and diffuse, hot gas. Some of the structures within this region, the Sickle HII region ionization front and photoevaporated pillars, in particular, suggest that gas is being collected and compressed (Cotera et al. 2006; Cotera et al. in preparation), and it morphologically resembles known regions outside the GC where such processes are believed to have led to the formation of a new generation of stars [e.g. M16; Smith, Stassun & Bally (2005)]. The energy injection from massive stars and possibly from the central supermassive black hole (SMBH), that is coincident with the radio source Sgr A*, may also strongly affect the thermal and/or dynamical properties of the ISM. Molecular gas in the GC, for example, has unusually high turbulent velocities and temperatures compared to clouds in other parts of the Galaxy (e.g. Morris & Serabyn 1996). This may bias the stellar initial mass function towards heavier stars and favour the production of massive star clusters (Morris 1993; Wang et al. 2006, and references therein).

To constrain the dynamical process of the known clusters, the overall population of massive stars and their formation modes, we sought to obtain a uniform survey of massive stars and their interplay with the ISM across the central 90 pc. Ionized warm gas provides the ideal tracer of massive stars and their interplay with their surroundings. Although previous radio continuum observations are free of extinction and trace both thermal and non-thermal emission, the scale dependence of radio interferometers makes it difficult to accurately measure flux densities on arcsecond scales. In addition, fine features (e.g. ionization fronts) are often found in the midst of diffuse non-thermal emission (e.g. the Radio Arc), making decomposition of thermal and non-thermal components challenging. Radio recombination line observations typically have a substantially lower signal-to-noise ratio and spatial resolution than radio continuum data. In the near-IR, the 2.16 μm Br$\gamma$ line is accessible from the ground (no suitable filter is available for existing and planned space-based platforms), but has also not proved effective for large-scale mapping of warm ionized gas. To our knowledge, no large-scale Br$\gamma$ line survey of the GC has ever been published. The difficulty lies in the lack of the combination of high spatial resolution and stable point spread function (PSF) in a ground-based survey. Observations with adaptive optics (AO) can have superb resolution, but only over small fields of view (typically 15–40 arcsec). The AO PSF also changes strongly, both spatially and with time, and has extended PSF wings, making the PSF subtraction extremely difficult. In addition, photometric conditions rarely, if ever, persist for the time required for such a survey, hampering the study of large-scale features.

We have carried out the first large-scale, high-resolution, near-IR survey of the GC, using *Hubble Space Telescope (HST)* NICMOS. The primary objective of the survey is to map out the hydrogen Paschen-$\alpha$ (P$\alpha$ for short) line (wavelength 1.876 μm) in a field of $\sim 39 \times 15$ arcmin$^2$ around Sgr A* (corresponding to $90 \times 35$ pc at the GC distance of 8 kpc; Ghez et al. 2008, Fig. 1). This field is known to be rich in clustered massive star formation (i.e. including the three known clusters). NICMOS observations of the P$\alpha$ emission were taken previously only for a few discrete regions, centred on the three known massive clusters (see Section 4.3 for further discussion). Our survey field also includes much unexplored territory. In particular, the region between Sgr A and Sgr C along the Galactic plane (to the right in Fig. 1) shows a number of compact *Spitzer* IRAC sources (several with radio counterparts) likely related to some of the earliest stages of massive star activities. This field selection also facilitates

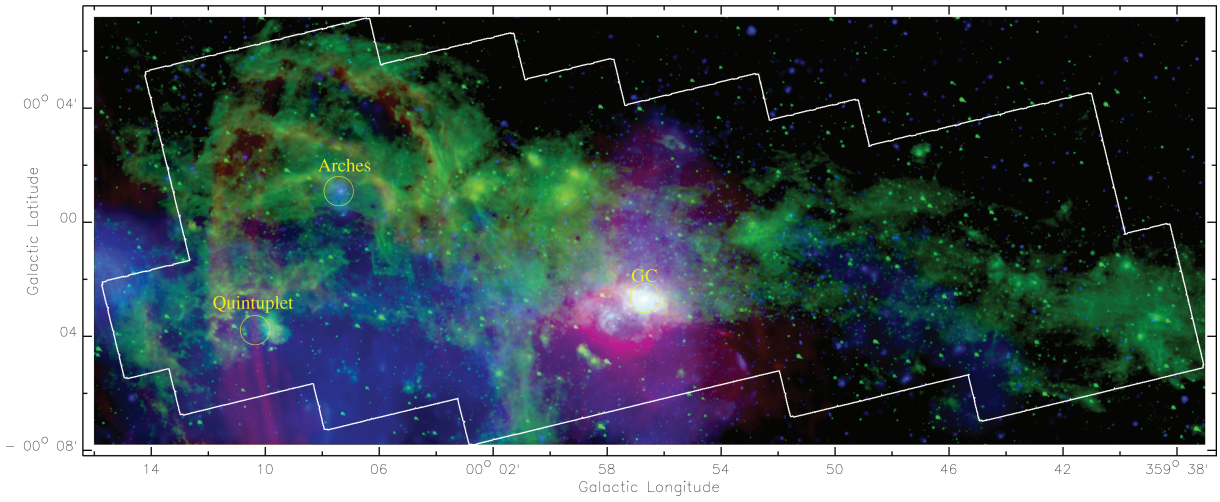


**Figure 1.** A multiwavelength montage of the GC: the Very Large Array 20-cm continuum (red; Yusef-Zadeh et al. 1984), *Spitzer* 8 μm (green; Stolovy et al. 2006; Arendt et al. 2008) and *Chandra* ACIS-I 1–9 keV (blue; Wang et al. 2002; Muno et al. 2009). The three known massive young clusters are shown, as well as the outer border of the P$\alpha$ survey.

an unbiased study of the apparent asymmetry between the positive and negative Galactic longitude sides relative to Sgr A*.

Our *HST* NICMOS observations overcome all of the potential problems of a ground-based survey. The wide NIC3 camera on this instrument provides a resolution of ∼0.2 arcsec with a stable PSF. This capability is important for detecting and cleanly removing point-like sources as well as resolving fine structures of extended features. Both the stable PSF and the absence of atmosphere for our *HST* survey mean that the entire survey is photometrically accurate and consistent. The extra magnitude of extinction along the sight-line to the GC at 1.87 μm (as compared to 2.16 μm) is more than compensated for by an intrinsic P$\alpha$ line intensity 12 times greater than the Br$\gamma$ line (Hummer & Storey 1987). In addition, the background at P$\alpha$ with NICMOS is a factor of ∼800 lower than the sky background at Br$\gamma$ as observed from the ground. This low background of *HST* NICMOS also allows us to detect faint point-like sources and extended features, particularly over our large mosaicked field.

## 2 OBSERVATIONS AND DATA REDUCTION

Our survey was completed in 144 *HST* orbits between 2008 February 22 and June 5. All of these orbits had an identical design, each consisting of 2 × 2 NIC3 pointing positions for both F187N (on-line) and F190N (off-line) filters. These filters have a 1 per cent bandpass centred at the wavelengths 1.875 and 1.900 μm. NIC3 is a 256 × 256 HgCdTe array detector with a pixel size of ∼0.2031 × 0.2026 arcsec$^2$ in the x- and y-directions. Adjacent positions and orbits were designed to have 3 arcsec overlaps in the vertical direction of the NIC3 array coordinates, partly to allow for the bottom 15 pixels that do not provide useful data due to afocal vignetting of that portion of the array. This is in addition to the overlaps resulting from the four-point dithers at each of the four positions of an orbit. Each dither exposure was taken in the MULTIACCUM readout mode (SAMP-SEQ = 16; NSAMP = 9) for photometry over a large flux range and for effective identification and removal of cosmic-rays and saturated pixels. The four-point dithers were in an inclined square wave pattern (i.e. the shifts were in the directions of 67.°5 relative to the *x*-axis of the detector coordinates); each dither step produced a shift of 2.33 and 5.63 arcsec pixels in the x- and y-directions. This dither pattern enabled both a sub-pixel sampling of the undersampled NIC3 PSF and a consistent overlap between orbits. Each orbit effectively covered an area of roughly 102 × 98 arcsec$^2$ (2.8 arcmin$^2$). With this strategy and a single telescope orientation, the survey mapped out a field of 416 arcmin$^2$ (as outlined in Fig. 1), and with a uniform 192 sec exposure per filter. The entire science data set includes 144 (orbits) × 4 (pointing positions) × 4 (dithers) × 2 (filters) = 4604 images.

In addition, between target visibility periods (during the Earth occultations) after each of the 144 orbits, 16 dark frames were obtained with the detector clocked in a manner identical to the science exposures. These inter-orbit raw dark exposures were assembled to form a 'superdark' frame used in our image calibration.

The data reduction and analysis, based on a combination of several newly developed tools and the standard routines implemented in the software IRAF/STSDAS, will be detailed in Dong et al. (in preparation). Briefly, in addition to the standard DC offset correction, we use a global fitting method to determine the relative instrumental background offsets among all NIC3 array quadrants, pointing positions, and orbits, based on multiple overlapping fields. A similar method is also used to optimize the correction for the relative astrometry offsets among orbits. The absolute astrometry is corrected with respect to radio counterparts of the near-IR sources in the field, reaching an accuracy better than 0.1 arcsec. The source detection is based primarily on the *StarFinder* software (Diolaiti et al. 2000).

The procedure and product of the data reduction are illustrated in Fig. 2 for global views and Fig. 3 for full-resolution close-ups. To estimate the continuum contribution in the F187N band (Figs 2a and 3a), we adaptively construct a mean F187N to F190N intensity ratio map, with the value of each pixel given as the median ratio of the nearest 100 sources, most of which are assumed to be located at the GC. However, this assumption does not hold for regions with exceptionally high extinction, as judged from a low surface number density of detected sources (i.e. $\lesssim 0.3$ sources arcsec$^{-2}$). For such regions, we calculate the ratio values from the extinction map obtained from *Spitzer* observations (see Dong et al., in preparation, for details; Schultheis et al. 2009). The continuum-subtracted map (Figs 2b and 3b) gives a crude look of the potential P$\alpha$-emitting sources as well as the diffuse emission. However, one cannot judge whether or not a peak (e.g. in Fig. 2b or 3b) is a P$\alpha$ emission source based only on its apparent excess above the background; such a peak can easily be caused by the statistical flux fluctuation of a subtracted source, especially a bright one. In fact, all peaks in 3b, except for the brightest one, are below our current P$\alpha$ source detection threshold. We identify P$\alpha$ source candidates based on their integrated continuum-subtracted fluxes at a statistical confidence $\gtrsim 5\sigma$, where $\sigma$ accounts for all known measurement errors (Dong et al., in preparation). To produce a *diffuse* P$\alpha$ map (Figs 2c and 3c), we use the actual F187N to F190N flux ratio of a detected source for its affected pixels (defined to have its PSF-predicted intensity contribution $\gtrsim 5\sigma$ above the local background in the F190N map). We further remove any uniformly distributed foreground and residual instrument background in a map by shifting its intensity to zero, averaged over a few darkest regions (see Section 3).

## 3 PRELIMINARY RESULTS

Fig. 2 shows a panoramic view of our survey data. Clearly, the distribution of both the stellar light and the diffuse emission is highly inhomogeneous, partly due to the variations in foreground extinction, which varies strongly from one region to another and on different spatial scales. The most outstanding extinction features in Fig. 2 are the distinct dark filaments (tendrils) in the field just above Sgr A, which are also noticeable in published *K*-band images (e.g. Philipp et al. 1999). The darkness of these filaments indicates that they are foreground thick dusty clouds silhouetted against the IR-luminous nuclear region of the Galaxy. The filaments appear to be structured down to arcsecond scales [or $\sim 10^{16}$ $(d/1\,\mathrm{kpc})$ cm, where $d$ is the distance to such a filament (see the full resolution close-ups in Fig. 3). With our data, we can distinguish between extinction and lack of ionized emission by comparing the P$\alpha$ and F190N images – if a region is dark in both images, we can say with confidence that the dark features indicate regions with extinctions $A_\mathrm{v} > 40$–50.

### 3.1 Extended P$\alpha$ Emission

Fig. 2(c) shows extended P$\alpha$-emitting complexes across much of the field. Strong and distinctive emission features are seen on angular scales from sub-arcsecond to about 10 arcmin, with surface brightness ranging from as high as ∼10 mJy (milliJansky) arcsec$^{-2}$ down to a 3$\sigma$ level of ∼0.05 mJy arcsec$^{-2}$ for the image with the 0.4 × 0.4 arcsec$^2$ pixel. The rms noise of a map depends on its pixel size and is ∼0.06 mJy arcsec$^{-2}$ for the full resolution image

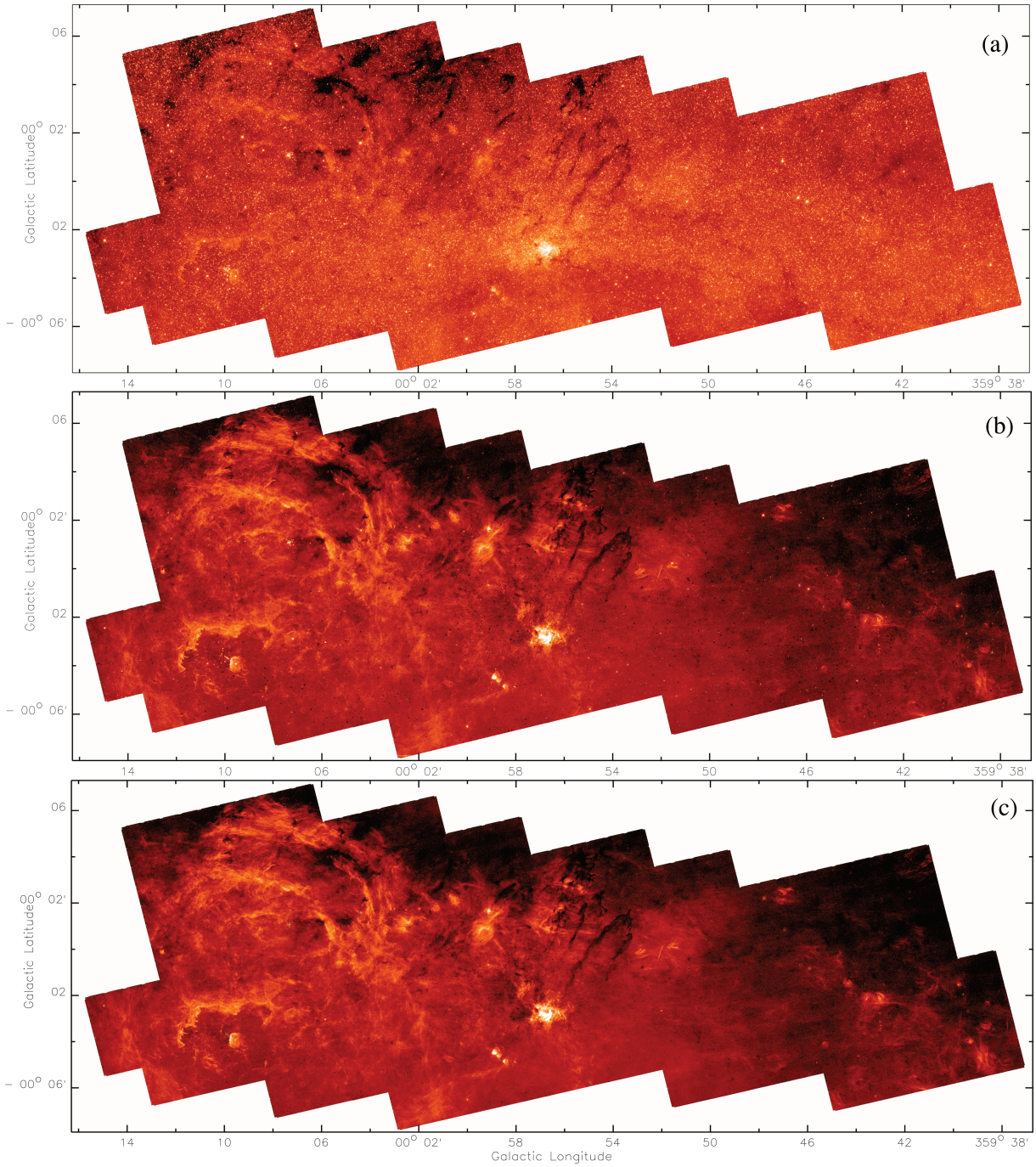


**Figure 2.** NICMOS maps from our survey: (a) calibrated F187N mosaic, (b) continuum-subtracted F187N map and (c) continuum-subtracted and point source removed F187N (diffuse P$\alpha$) map. These maps are presented with a bin size of 0.4 arcsec. The intensity is logarithmically scaled from 0.01 to 10 mJy arcsec$^{-2}$ in (a) and to 3 mJy arcsec$^{-2}$ in (b) and (c).

with a pixel size of 0.1 × 0.1 arcsec$^2$, accounting for both statistical and systematic fluctuations (photon counting, artefacts from stellar continuum subtraction, etc.). This noise is estimated from selected regions in the P$\alpha$ map [e.g. at the upper right corner of the map; see Dong et al. (in preparation) for details] that show little P$\alpha$ emission but are bright in the F190N continuum image (hence the rms contribution from clumpy structures in the P$\alpha$ emission or extinction should be minimal). The overall distribution of the P$\alpha$ emission is highly lopsided towards the positive Galactic longitude side of the GC, similar to what is seen in radio and mid-IR (Fig. 1).

The diffuse P$\alpha$ emission is greatly enhanced around the three known clusters responsible for the ionization of the inner rims of surrounding gas. The emission around the GC cluster is largely confined within a small spiral-like nuclear structure, the P$\alpha$ emission of which was first detected by Scoville et al. (2003). Our new survey now enables us to trace the faint emission features to large distances, which extend vertically below and above this structure (Fig. 4a). These features may represent outflows from the central few parsec of the galaxy. The bright P$\alpha$ emission itself indicates the ionized inner portion of a dusty circumnuclear disc around Sgr A*. This disc

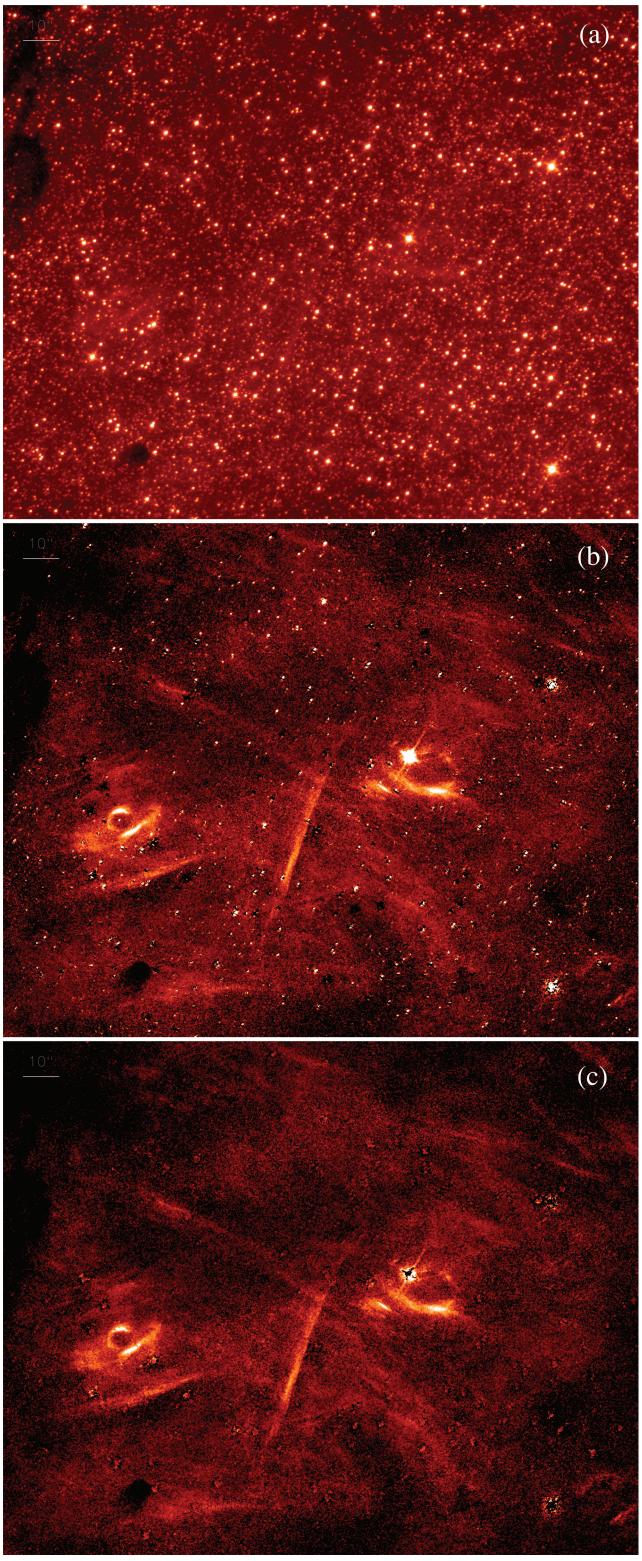


**Figure 3.** A full-resolution (0.1 arcsec pixel) close-up of a newly discovered P$\alpha$-emitting complex (G359.866+0.002), about 5 arcmin northwest of Sgr A*: (a) F187N image, (b) continuum-subtracted F187N image and (c) point source removed (diffuse P$\alpha$) image. The intensity is logarithmically scaled over the range 0.1–30 mJy arcsec$^{-2}$ in (a) and 0.1–1 mJy arcsec$^{-2}$ in (b) and (c).

appears more extended, as traced by the 8 μm emission (Fig. 4a). A detailed analysis/modelling of these structures is needed to further investigate the physical state of the disc and the energetics of the GC cluster and/or the SMBH, which is currently in a radiatively inefficient accretion state.

Fig. 4(b) presents a close-up of the Sickle H II region, revealing fingers of ionized gas resembling the 'Pillars of Creation' in M16 (Cotera et al. 2006). These fingers are apparently illuminated by ionizing photons from hot stars in the Quintuplet cluster (Cotera et al. 2006; Simpson et al. 1997, Cotera et al., in preparation). The P$\alpha$-emitting 'Arches' around the Arches cluster show an amazing array of fine linear structures (Fig. 4c), which are preferentially oriented in the same directions as magnetic field vectors measured in infrared polarization (Chuss et al. 2003; Nishiyama et al. 2009). Similar, organized narrow linear P$\alpha$-emitting features are also abundant in some of the more compact H II regions seen in Fig. 2(c). These structures may indicate a critical role that locally strong magnetic fields play in shaping the morphology and dynamics of the ionized gas (e.g. Nishiyama et al. 2009).

Fig. 5 shows a selection of compact P$\alpha$-emitting nebulae. Some of these enigmatic nebulae may represent individual massive stars in formation (e.g. the first row in Fig. 5), whereas others may be due to stellar ejecta and/or their interaction with dense ambient medium (the second and third rows).

### 3.2 Point-like sources

The survey also enables us to perform an unprecedentedly uniform, high-resolution, photometrically sensitive census of the stellar population. Our preliminary detection based on the F190N continuum image gives a total of about 0.6 million point-like sources, which accounts for about 86 per cent of the total observed F190N intensity in the survey field. The median of the unresolved intensity is $\sim$0.04 mJy arcsec$^{-2}$, averaged over the surveyed field. Our 50 per cent source detection limit is about 17th mag in the F190N band. A preliminary analysis shows that we should detect most of the massive main-sequence stars (earlier than B3, corresponding to $\sim$8 $M_{\odot}$) in the region as well as the bulk of red giants, including red clump stars. A detailed analysis of the spatial distribution of the detected sources and the still unresolved intensity will allow us to infer the overall intrinsic structure of the stellar light distribution in the GC and to provide quantitative measurements of the foreground extinction.

Our preliminary analysis has resulted in the detection of about 200 P$\alpha$-emitting star candidates. Before the publication of such candidates, however, we still need additional careful examination, especially for relatively weak sources, to minimize potential systematic contamination (e.g. due to local enhancements of diffuse P$\alpha$ complexes). We easily detect all previously known emission-line stars throughout the survey region ($\sim$70 in total, mostly Wolf–Rayet stars). We have already verified an additional 30 emission-line stars via spectroscopic follow-up observations (Mauerhan et al. 2009, Cotera et al. in preparation). We anticipate that further follow up observations will at least double that number again. More importantly, over half of the newly identified stars are located outside the three known clusters. Therefore, we have already more than doubled the number of known intercluster emission-line stars. The newly discovered stars will enable us to address in greater detail the formation of massive stars outside clusters in our upcoming papers. In particular, the P$\alpha$ star candidates outside the clusters are not distributed in a completely random fashion. In addition to the P$\alpha$ emission line, the F187N filter contains a few helium lines which

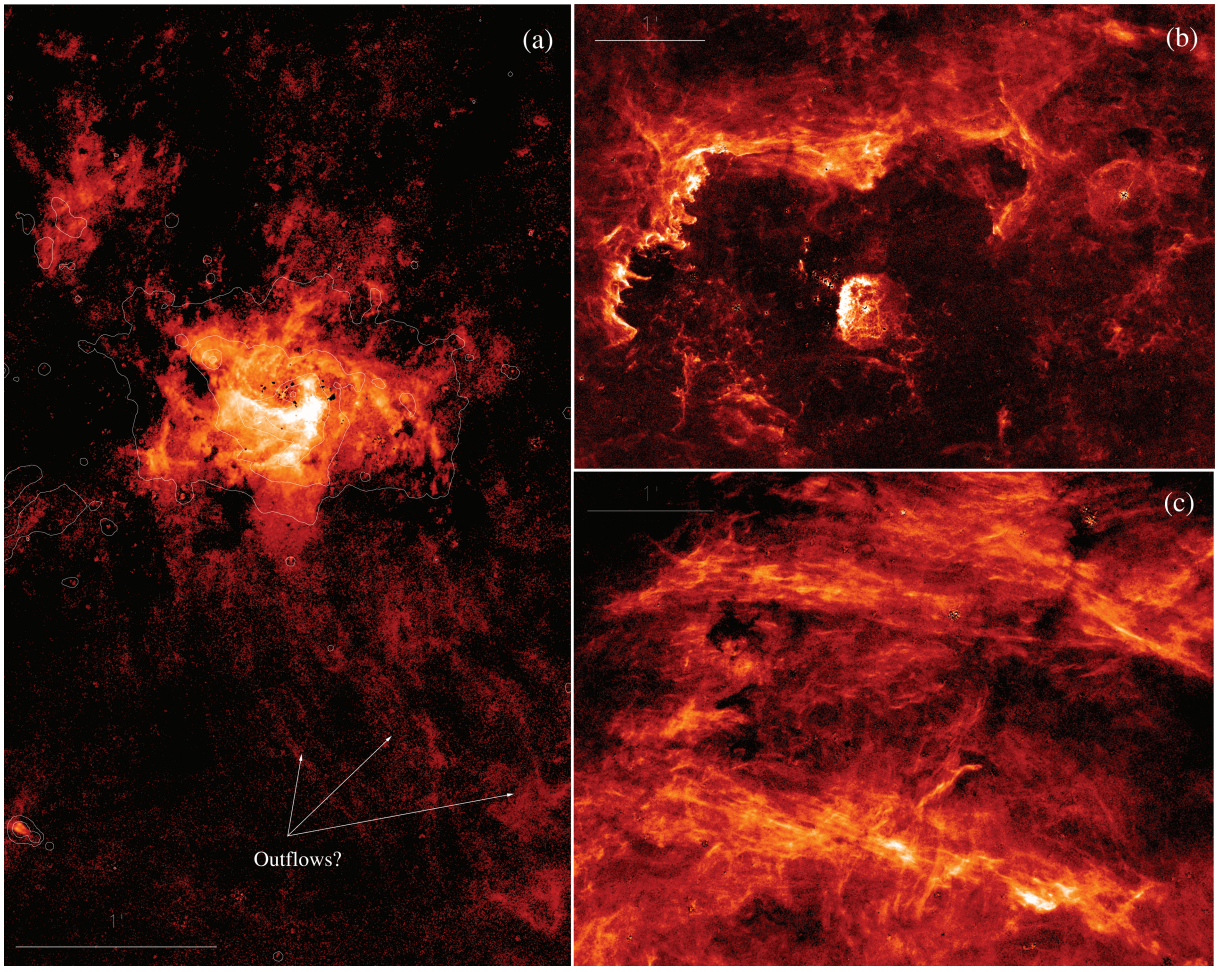


**Figure 4.** Close-ups of the P$\alpha$-emitting features: (a) the central region around Sgr A$*$, with overlaid IRAC 8 μm intensity contours at 1, 3, 10 and $30 \times 10^3$ mJy sr$^{-2}$; (b) the Sickle nebula [G0.18−0.04; e.g. (Lang, Goss & Wood 1997)] and (c) thermal Arched filaments (e.g. Lang, Goss & Morris 2001). All are projected in the Galactic coordinates.

are often strong emission lines in Wolf–Rayet stars. Therefore, the most easily detected stars in the F187N filter are typically Wolf–Rayet stars, although future refinements to the data analysis will enable us to detect O and possible B supergiants as well, which have smaller P$\alpha$ equivalent widths, in emission or absorption. Such refinements may be achieved by modelling the broad-band spectral energy distribution together with the narrow band measurements of the P$\alpha$ emission and absorption.

## 4 DISCUSSION

While the data analysis, multi-wavelength comparison, follow-up observations and modelling are still ongoing and will be presented in later papers, we discuss here the implications of the survey for addressing several key issues related to star formation and its impact on the GC environment:

### 4.1 How do massive stars form in the GC?

Two large questions remain unanswered about massive star formation in the GC: (1) Do massive stars form exclusively in the clusters, or in looser associations throughout the field? (2) Is star formation continuous, or does it happen in discrete bursts? Until recently, massive (e.g. emission line) stars have mostly been found within the three GC clusters. A number of searches for young massive stars at infrared and X-ray wavelengths have been carried out (e.g. Cotera et al. 1999; Muno et al. 2006a; Mauerhan et al. 2007, 2009). These studies, each with diverse search criteria, have yielded a rather incomplete picture of the young massive star population in this GC.

The P$\alpha$ emission is a sensitive tracer of massive stars and their environs. The emission traces warm ionized gas, produced and maintained primarily by Lyman continuum radiation from massive stars. Such gas can be associated with individual stars (e.g. massive stellar winds), their immediate vicinities (circumstellar material) and surrounding ISM structures. The fact that the majority of our new sources are actually located outside the three known clusters has strong implications for understanding the dynamics of massive stars with ages of only a few $\times$ 10$^6$ yr. The exact time-scales for clusters to be disrupted and the place where the stars end up provide information about the internal dynamics of the clusters as well as the large-scale tidal force of the GC (Kim et al. 1999; Kim et al. 2000; Portegies Zwart et al. 2002; Kim & Morris 2003; Portegies Zwart, McMillan & Gerhard 2003; Kim, Figer & Morris 2004). The spatial distribution of the massive stars detected in our survey can be used to better constrain these processes throughout the field. The distributions of the stars and their types as well as follow-up work on both radial velocities and proper motions (Stolte et al. 2008) will

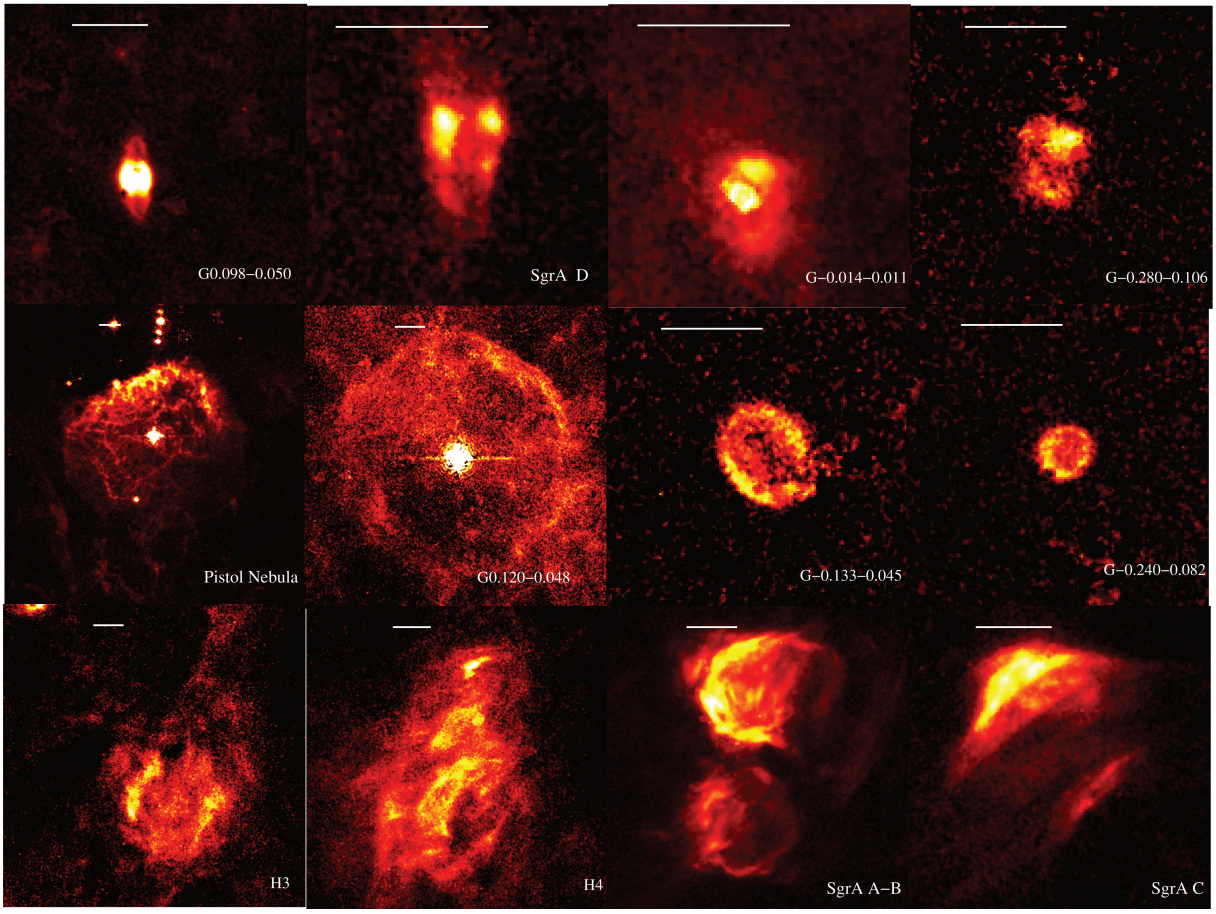


**Figure 5.** Close-ups of P$\alpha$ images of selected individual nebulae (equatorially projected). Detected sources have been subtracted, except for identified bright P$\alpha$ emission star candidates, which help to show their potential relationship to the corresponding nebulae. The nebulae are labelled with rough Galactic coordinates, except for those with well-known names. The bar in each panel marks a 0.2 pc scale at the GC distance.

allow us to constrain how quickly the massive stellar clusters are currently dissolving, how many star clusters have been disrupted and whether or not the stars are formed in massive clusters which have been subsequently dispersed or formed in relative isolation.

### 4.2 What are the state and dynamics of the ISM?

In the high-pressure and high-density environment of the GC, the diffuse P$\alpha$-emitting gas tends to be found at ionization fronts bordering molecular clouds. The gas density and pressure are expected to change drastically at such fronts (e.g. Scowen et al. 1998). The high-resolution P$\alpha$ map resolves various ionization fronts, which helps to determine the local neutral gas density and the thermal pressure of diffuse warm ionized gas. The comparison between Figs 1 and 2 demonstrates the complicated relationship among various stellar and ISM components. Within the Sickle region (Fig. 4b), for instance, we see two distinctive ionization front morphologies. We see columns of photo-evaporating gas similar to the elephant trunks or pillars seen in regions such as M16 in one part, but also a remarkably smooth ionization front located on another side of the large H II region. Although very different, both are morphologically perpendicular to the brightest non-thermal radio filaments, which are uniquely found in the GC field and have been a longstanding mystery. They are known to trace enhanced magnetic field and/or cosmic rays. But the underlying physical processes remain unclear. The observed relative morphological configuration then suggests that the large-scale, inter-cloud, vertical (poloidal) magnetic field is combing through the dense gas and gets enhanced in the process. The expansion of the magnetized inter-cloud material, probably accompanied with cosmic ray acceleration, is likely driven by the strong mechanical energy output from the Quintuplet and Arches clusters, consistent with the barrel-shaped morphology of the non-thermal radio filaments (Fig. 1). Therefore, the feedback from the clusters likely plays an important role in shaping the ISM and the eco-system of the GC in general.

### 4.3 Comparison with other observations

A few P$\alpha$ observations were made previously in the GC region. The Sgr A West region, covering the inner $\sim$4 pc of the Galaxy, was observed using both NIC3 and NIC2 (e.g. Scoville et al. 2003). Several other programs concentrated only on the central parsec with NIC1. A NIC2 P$\alpha$ observation was also made for the core of the Arches cluster (Figer et al. 2002). The P$\alpha$ emission from the Pistol Nebula (Fig. 4b) was covered with a 2 $\times$ 2 mosaic of NIC2 observations, which had a smaller field of view (19.2 arcsec on a side; Figer et al. 1999). Our map shows considerably more structure in the diffuse P$\alpha$ emission of the Nebula than the image shown in Figer et al. (1999), apparently due to the higher sensitivity of our NIC3 observations. In addition, our new data provide additional epochs for variability analysis in these regions with the existing observations (e.g. Blum et al. 2001).

 

Our study of the GC region complements other efforts to understand Galactic star-forming regions, such as Orion (e.g. Feigelson et al. 2005), the Carina nebula (e.g. Tapia et al. 2006), NGC 3603 (Stolte et al. 2004, 2006) and Westerlund 1 (e.g. Muno et al. 2006b). It is crucial to compare the time-scales and efficiency with which stars form in the GC to those in other regions of the Galactic disc in order to gain a detailed understanding of the interplay between massive stars and the ISM.

Ultimately, understanding the gas removal, via the formation of massive stars and their impact on the ISM or other processes (e.g. Type Ia supernova-driven Galactic bulge wind; Tang et al. 2009; Li, Wang & Wakker 2009), will help to determine why some host SMBHs accrete at rates near their Eddington limits, while others, including Sgr A*, are at rates orders of magnitude lower.

## ACKNOWLEDGMENTS

We gratefully acknowledge the support of the staff at STScI for implementing the survey and for helping in the data reduction and analysis. Support for program HST-GO-11120 was provided by NASA through a grant from the Space Telescope Science Institute, which is operated by the Association of Universities for Research in Astronomy, Inc., under NASA contract NAS 5-26555.

## REFERENCES

Arendt R. G. et al., 2008, ApJ, 682, 384
Blum R. D., Schaerer D., Pasquali A., Heydari-Malayeri M., Conti P. S., Schmutz W., 2001, AJ, 122, 1875
Chuss D. T., Davidson J. A., Dotson J. L., Dowell C. D., Hildebrand R. H., Novak G., Vaillancourt J. E., 2003, ApJ, 599, 1116
Cotera A. S., Erickson E. F., Colgan S. W. J., Simpson J. P., Allen D. A., Burton M. G., 1996, ApJ, 461, 750
Cotera A. S., Simpson J. P., Erickson E. F., Colgan S. W. J., Burton M. G., Allen D. A., 1999, ApJ, 510, 747
Cotera A. et al., 2006, J. Phys. Conf. Ser., 54, 183
Diolaiti E., Bendinelli O., Bonaccini D., Close L. M., Currie D. G., Parmeggiani G., 2000, in Wizinowich P. L., ed., Proc. SPIE 4007, Adaptive Optical Systems Technology. SPIE, Bellingham, p. 879
Feigelson E. D. et al., 2005, ApJS, 160, 379
Figer D. F., Morris M., Geballe T. R., Rich R. M., Serabyn E., McLean I. S., Puetter R. C., Yahil A., 1999, ApJ, 525, 759
Figer D. F. et al., 2002, ApJ, 581, 258
Genzel R. et al., 2003, ApJ, 594, 812
Ghez A. M. et al., 2008, ApJ, 689, 1044
Hummer D. G., Storey P. J., 1987, MNRAS, 224, 801
Kim S. S., Morris M., 2003, ApJ, 597, 312
Kim S. S., Morris M., Lee H. M., 1999, ApJ, 525, 228
Kim S. S., Figer D. F., Lee H. M., Morris M., 2000, ApJ, 545, 301
Kim S. S., Figer D. F., Morris M., 2004, ApJ, 607, L123
Lang C. C., Goss W. M., Wood D. O. S., 1997, ApJ, 474, 275
Lang C. C., Goss W. M., Morris M., 2001, AJ, 121, 2681
Li Z. Y., Wang Q. D., Wakker B., 2009, MNRAS, 397, 148
Mauerhan J., Muno M., Morris M. R., 2007, ApJ, 662, 574
Mauerhan J., Muno M. P., Morris M. R., Bauer F. E., Nishiyama S., Nagata T., 2009, ApJ, 703, 30
Morris M., 1993, ApJ, 408, 496
Morris M., Serabyn E., 1996, ARA&A, 34, 645
Muno M., Bower G. C., Burgasser A. J., Baganoff F. K., Morris M. R., Brandt W. N., 2006a, ApJ, 638, 183
Muno M. P., Law C., Clark J. S., Dougherty S. M., de Grijs R., Portegies Zwart S., Yusef-Zadeh F., 2006b, ApJ, 650, 203
Muno M. P. et al., 2009, ApJS, 181, 110
Nishiyama S. et al., 2009, ApJ, 690, 1648
Philipp S., Zylka R., Mezger P. G., Duschl W. J., Herbst T., Tuffs R. J., 1999, A&A, 348, 768
Portegies Zwart S. F., Makino J., McMillan S. L. W., Hut P., 2002, ApJ, 565, 265
Portegies Zwart S. F., McMillan S. L. W., Gerhard O., 2003, ApJ, 593, 352
Schultheis M., Sellgren K., Ramírez S., Stolovy S., Ganesh S., Glass I. S., Girardi L., 2009, A&A, 495, 157
Scoville N., Stolovy S. R., Rieke M., Christopher M., Yusef-Zadeh F., 2003, ApJ, 594, 294
Scowen et al., 1998, AJ, 116, 163
Serabyn E., Shupe D., Figer D. F., 1998, Nat, 394, 448
Simpson J. P., Colgan S. W. J., Cotera A. S., Erickson E. F., Haas M. R., Morris M., Rubin R. H., 1997, ApJ, 487, 689
Smith N., Stassun K. G., Bally J., 2005, ApJ, 129, 888
Stolovy S. et al., 2006, J. Phys. Conf. Ser., 54, 176
Stolte A., Brandner W., Brandl B., Zinnecker H., Grebel E. K., 2004, AJ, 128, 765
Stolte A., Brandner W., Brandl B., Zinnecker H., 2006, AJ, 132, 253
Stolte A., Ghez A. M., Morris M., Lu J. R., Brandner W., Mathews K., 2008, ApJ, 675, 1278
Tang S. K., Wang Q. D., Lu Y., Mo H. J., 2009, MNRAS, 392, 77
Tapia M., Persi P., Bohigas J., Roth M., Gómez M., 2006, MNRAS, 367, 513
Wang Q. D., Gotthelf E., Lang C. C., 2002, Nat, 415, 148
Wang Q. D., Dong H., Lang C. C., 2006, MNRAS, 371, 38
Yusef-Zadeh F., Morris M., Chance D., 1984, Nat, 310, 557
Yusef-Zadeh F., Law C., Wardle M., Wang Q. D., Fruscione A., Lang C. C., Cotera A., 2002, ApJ, 570, 665

This paper has been typeset from a TEX/LATEX file prepared by the author.